Journal of Environmental Chemical Engineering 10 (2022) 108718

Contents lists available at ScienceDirect

Journal of Environmental Chemical Engineering

journal homepage: www.elsevier.com/locate/jece

Glutathione assisting the waste tobacco leaf to synthesize versatile biomass-based carbon dots for simultaneous detection and efficient removal of mercury ions

Hui Yang [a,b,c], Xiankun Su [a], Li Cai [d], Zhenchun Sun [a], Yechun Lin [a], Jing Yu [a], Likai Hao [b,*], Cui Liu [e,*]

[a] Guizhou Academy of Tobacco Science, Guiyang 550081, China
[b] State Key Laboratory of Environmental Geochemistry, Institute of Geochemistry, Chinese Academy of Sciences, Guiyang 550081, China
[c] University of Chinese Academy of Sciences, Beijing 100049, China
[d] Guizhou Tobacco Quality Supervision and Measure Station, Guiyang 550081, China
[e] Institute of Medical Engineering, Department of Biophysics, School of Basic Medical Sciences, Xi'an Jiaotong University Health Science Center, Xi'an 710061, China

ARTICLE INFO

Editor: Dr Xianwei Liu

Keywords:
Waste tobacco leaf
Red fluorescence biomass-based CDs
Hg^{2+}
Detection and removal
Large Stokes shift emission

ABSTRACT

High-efficient conversion of the waste biomass into eco-friendly novel bifunctional materials for selective monitoring and effective removal of mercury ions (Hg^{2+}) is of great significance to achieve the environment sustainable development, but has not attracted enough attention. Herein, we exploited glutathione (GSH) assisting waste tobacco leaf as the biomass-related precursors to successfully yield a novel red fluorescence emission biomass-based carbon nanodots (CDs) with a remarkably large Stokes shift of ~ 232 nm through one-pot hydrothermal method. Owing to the synergistic Hg-S bond and the coordination effects of the Hg^{2+} to the abundant –COOH, $–NH_2$ and –OH groups on the surface of CDs, this proposed biomass-based CDs showed a red fluorescence decrease response for Hg^{2+} with a high selectivity and a lower detection limit of 0.45 μM in environmental water samples. Furthermore, this binding endowed this proposed biomass-based CDs possessed a high removal efficiency of above 99.4% for Hg^{2+} as well. This work showed a novel insight into recycling the waste tobacco leaf into novel, economic, efficient, reliable, and eco-friendly biomass-based CDs for simultaneously precise traceability and high-efficient removal of Hg^{2+} pollution in environmental matrices.

1. Introduction

As a typical heavy metal pollutant, the residual mercury ion (Hg^{2+}) poses a serious threat to environmental health and food safety, because it possesses high toxicity even at very low level [1-3]. In particular, with the rapid development of economy and society, various production activities lead to more and more serious Hg^{2+} pollution in the surface water and environmental water, thereby being ingested into human body with the food chain cycle [4]. It has been proved that the long-term exposure to Hg^{2+} pollution will cause a series of side effects, such as brain damage, insomnia, cognitive and motor impairments [5,6]. Therefore, it is of great significance to develop an efficient material for achieving the simultaneous monitoring and removal of Hg^{2+} in water resources. Driven by this motivation, until now, vast efforts have been contributed to employ metal organic frameworks (MOFs) [7,8], covalent organic frameworks (COFs) [9,10], $MoSe_2$ nanosheet [11], mesoporous silica-based nanomaterials [12], or polymers [13,14] as the substrates for successful achieving the simultaneous detection and removal of Hg^{2+}. However, several unavoidable drawbacks seriously restrict their popular applications. For example, the MOFs generally suffer from poor stability, while COFs have bad solubility [15,16]. Meanwhile, the preparation process of $MoSe_2$ nanosheet involves the utilization of organic solvents, which breaches the purpose for ecological security. Likewise, mesoporous silica-based nanomaterials or polymers need complicated molecular design and time-consuming synthesis process. In view of this situation above, more efforts are needed to continue to explore stable and soluble novelty materials for simultaneous monitoring and removal of Hg^{2+} in simple, environmentally friendly, efficient way.

As a new type of fluorescent nanomaterials, carbon nanodots (CDs)

* Corresponding authors.
E-mail addresses: haolikai@mail.gyig.ac.cn (L. Hao), liucui@xjtu.edu.cn (C. Liu).

https://doi.org/10.1016/j.jece.2022.108718
Received 3 August 2022; Received in revised form 30 September 2022; Accepted 4 October 2022
Available online 12 October 2022

have attracted tremendous attention due to their exceptional optical properties (Manikandan V and Lee, 2022). At present, CDs are mainly prepared from chemical materials (small molecules, polymers) or biomass (plant, and animal derivatives, etc.) through different ways of carbonization [17,18]. Common methods include hydrothermal, solvothermal or microwave assisted hydrothermal/ solvothermal and so on [19]. Both CDs prepared from commercial chemicals and biomass have the advantages of small particle size, easy synthesis and good water solubility [20-23,17]. Compared with CDs prepared from commercial chemicals, the raw material of biomass-based CDs is environment-friendly natural products, which has the advantages of low cost, easy availability, green, and large quantity. Recently, the waste resources-derived biomass-based CDs has inspired intensive research in environment monitoring and treatment, because of its good properties such as turning "waste" into "treasure", low cost, and eco-friendly [24-27]). Given these excellent features, in combination with the aim on the renewable utilization and sustainable development demand, the waste resources-derived biomass-based CDs might be a prominent candidate for co-friendly simultaneous monitoring and removal of Hg^{2+} in water resources. Up to now, several biomass-based CDs derived from the waste potato peels [28], bee pollen [26], tree leaves [29,30], *Poa pratensis* [31], corn stalk shell [9,32,33], and peanut shells [34] have been reported for detection of different analytes. A typical example was that Liu et al. used waste sweet potato peels to synthesize fluorescent biomass-based CDs to perform the precise detection of tetracycline analogues [28]. Subsequently, Shan et al. extracted bee pollen waste to prepare another biomass-based CDs that were able to allow the sensing of Fe^{3+} environmental water through the coordination effect of Fe^{3+} toward the functional groups on the surface of CDs [26]. Lately, Li's group exploited the waste *Poa pratensis* to propose a novel *N*-doped biomass-based CDs for successful achieving the simultaneous of Fe^{3+} and Mn^{2+} in water samples, owing to the coordination effect of the CDs with Mn^{2+} & Fe^{3+} as well [31]. From these cases, no concerns have been focused on developing the waste resources-derived biomass-based CDs to carry out the simultaneous monitoring and removal of Hg^{2+}, even it fits well with the environmental conservation and sustainable development strategies.

Enlightened by these points above, we herein concentrated on exploring the waste resources to synthesize the versatile novelty biomass-based CDs for yielding the detection and elimination of Hg^{2+} in a simple, precise, reliable, economic, and eco-friendly way. For this purpose, we applied a one-pot hydrothermal method to synthesize a novel waste tobacco leaf-derived biomass-based CDs upon the assistance of GSH. Through in-depth analysis, this proposed biomass-based CDs displayed a red fluorescence with emission wavelength of ~ 652 nm with a remarkable Stokes shift of ~ 232 nm. It has been reported that the integration of the large Stokes shift and red emission is beneficial to yield the more sensitive fluorescence assay toward the targeting analytes in complicated conditions with low background auto-fluorescence interference [35,36], Yizhong, Tingting et al., 2020). Additionally, the biomass-based CDs showed a strong and selective binding ability toward Hg^{2+} to form the ground-state complex Hg^{2+}-CDs, because of the synergistic Hg-S bond and the coordination effects of the Hg^{2+} to the abundant –COOH, $–NH_2$ and –OH groups on the surface of CDs. As expected, the NIR fluorescent of CDs at ~ 652 nm was quenched, allowing for the fluorescence assay for Hg^{2+}. More significantly, this binding ability of the proposed biomass-based CDs to Hg^{2+} could be applied for achieving the effective removal of Hg^{2+} in contaminated water with a high efficiency of 99.4 % (Scheme 1). This work revealed the promising practical potentials of the waste tobacco leaf-derived biomass-based CDs in Hg^{2+} pollution traceability, control and remediation in an efficient, low-cost, and eco-friendly way.

2. Materials and methods

2.1. Materials and reagents

Waste tobacco leaf was obtained from the Guizhou Academy of Tobacco Science. Glutathione (reduced) (GSH), formamide, sodium acetate, citric acid, and dimethyl sulfoxide (DMSO) were purchased from Sinopharm Chemical Reagent Co. China. Barium chloride ($BaCl_2$), 1,4-dioxane, 4-sulfophenyl isothiocyanate (SPI) sodium salt monohydrate, 1,3-propane sultone (PS), ferric chloride ($FeCl_3$), strontium chloride ($SrCl_2$), magnesium sulphate ($MgSO_4$), calcium sulphate ($CaSO_4$), cobalt chloride ($CoCl_2$), tin chloride ($SnCl_2$), lead acetate ($(CH_3COO)_2Pb$), copper sulphate ($CuSO_4$), manganese sulphate ($MnSO_4$), zinc sulphate

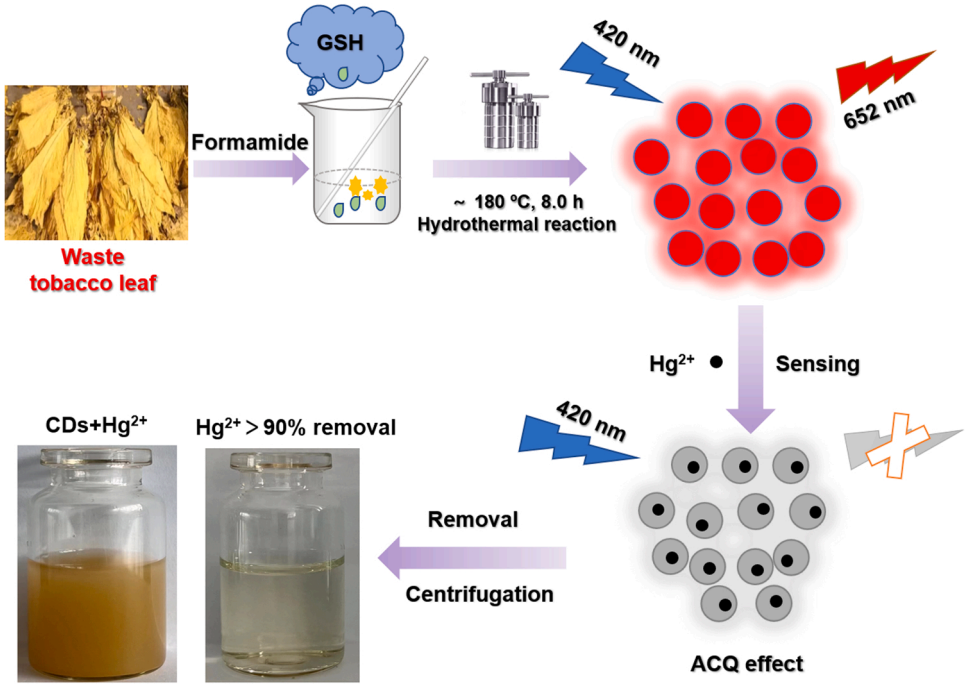

Scheme 1. The synthesis of this biomass-based CDs and schematic illustration for detection and removal of Hg^{2+}.

($ZnSO_4$), mercury sulphate ($HgSO_4$), platinum chloride ($PtCl_4$), palladium nitrate ($Pd(NO_3)_2$), aluminium chloride ($AlCl_3$), vanadium chloride (VCl_3), chromium chloride (VCl_2), nickel chloride ($NiCl_2$), cadmium chloride ($CdCl_2$), and silver nitrate ($AgNO_3$) were purchased from Shanghai Aladdin Biochemical Technology Co. China. All chemical reagents were used as received. Ultrapure water (Millipore) was used throughout the experiments.

2.2. Apparatus

The absorption spectra of the samples were taken on a Carry 50 UV–vis absorption spectrometer (UV–vis); fluorescence spectra were taken on an F-7000, and transmission electron microscopy (TEM) images were taken using a Tecnai G2 F20 S-TWIN (200 kV). Fourier transform infrared spectroscopy (FT-IR) was conducted on a Nicolet iS10 using the KBr compression method; and X-ray photoelectron spectroscopy (XPS) was conducted on a Thermo Fisher Scientific ESCALAB 250Xi photoelectron spectrometer. X-ray diffraction (XRD) experiments were conducted on a BRUCKER D8. Raman spectroscopy was performed using a Renishaw inVia Raman microscope. Hydrogen spectrum nuclear magnetism (^{1}H NMR) were used to characterize the composition and surface functional groups of this biomass-based C-dots. Fluorescence decay curve was measured using a steady-state, transient fluorescence JY HORIBA Fluorolog-3. The absolute quantum yield of the as-synthetized biomass-based CDs was measured by Edinburgh FLS9 (Ex:420 nm at room temperature).

2.3. Synthesis of CDs

For the synthesis of CDs, 0.25 g waste tobacco leaf powder was mixed with 0.30 g GSH and 10.0 mL of formamide. The reaction was then carried out in a muffle furnace at 180.0 °C for 8.0 h. Next, the mixture was centrifuged at 4000 rpm for 30.0 min and filtered through a filter membrane (0.22 μm). The obtained dark green filtrate was transferred to a dialysis bag (3500 Dalton) and dialyzed for 7 days. The solution was then freeze-dried to obtain powder samples.

2.4. Determination and removal of Hg^{2+}

2.0 mL 12.5 μg/mL CDs (dissolved in pH 6.8 B-R buffer) solution and 2.0 mL of Hg^{2+} solution containing different concentrations were placed into a 5.0 mL centrifuge tube, mixed thoroughly, and then left for 30.0 min at room temperature to determine the fluorescence spectra. The excitation wavelength was 420 nm, and the slit widths for both excitation and emission were 5.0 nm. A total of 20.0 ions, including Al^{3+}, Ba^{2+}, Ca^{2+}, Cd^{2+}, Co^{2+}, Cu^{2+}, Fe^{3+}, Mg^{2+}, Mn^{2+}, Ni^{2+}, Zn^{2+}, V^{3+}, V^{2+}, Sr^{2+}, Sn^{2+}, Pt^{4+}, Pd^{2+}, Pb^{2+}, Ag^{+}, and Hg^{2+} were selected to examine for the selectivity of this biomass-based CDs to detect Hg^{2+}.

In a 1.5 mL centrifuge tube,500.0 μL 100.0 μmol/L of Hg^{2+} solution was added into 500.0 μL 100.0 μg/mL CDs solution, mixed thoroughly, reacted in a B-R buffer pH 6.8 for 30.0 min at room temperature. The mixture solution was centrifuged at 10000 rpm for 10.0 min. The supernatant and the precipitate were then taken for a Hg^{2+} concentration test by ICP-AES.

2.5. Testing of actual samples

Pond water, lake water, and tap water were randomly collected from the Karst Park, Yueshanhu Park, and the laboratory faucet (Guiyang, China), respectively. The tap water was used without any pre-treatment. The pond water and lake water were centrifuged (4000.00 rmp, 15.0 min) and filtered through a 0.22 μm filter to remove the probably suspended particles.

2.5.1. Detection of Hg^{2+} in tap and lake water

The application of the established method to tap and lake water was investigated by the spiking method. 1.5 mL lake water and 1.5 mL tap water were added to 1.5 mL 12.5 μg/mL CDs solution, respectively. The solutions were thoroughly mixed and incubated for 30.0 min at room temperature. Finally, the fluorescence emission spectra were measured at 420 nm excitation wavelength.

2.5.2. Removal of Hg^{2+} from pond water samples

The pond water was applied to investigate the practicality of this biomass-based CDs to removal of Hg^{2+}. The removal experiment was carried out at room temperature. In detail, $HgSO_4$ standard solution were spiked in the water sample to obtained 60.0–200.0 μM spiking level. Then 1.5 mL above Hg^{2+} spiking water samples were mixed with 1.5 mL 100 μg/mL CDs, respectively. After reaction for 30.0 min, the Hg^{2+}-CDs complexes were separated from the mother liquor by centrifugation. Next, the content of residual Hg^{2+} in the supernatant was determined by ICP-AES. Finally, the removal efficiency of CDs on Hg^{2+} was calculated as follows: removal efficiency (%) = $(C_0\text{-}C)/C_0$, where C_0 and C are the initial concentration of Hg^{2+} added and the concentration of residual ion in the supernatant, respectively.

2.6. Cell viability assay

Human cervical carcinoma HeLa cells were selected as the model to assess the environmental safety of this biomass-based CDs through exploring its effect toward cell viability. The HeLa cells were cultured with Dulbecco's modified Eagle's medium (DMEM, 10.0 % fetal bovine serum, 100.0 mg/L streptomycin, and 100.0 U/mL penicillin) at 37.0 °C in a humidified incubator containing 5.0 % CO_2 and 95.0 % air. For performing the cell viability assay, ~ 5000 HeLa cells were planted into a 96-well plate to culture in 100.0 μL fresh DMEM medium for 24.0 h in the humidified incubator. Then, the medium in each well was carefully replaced with 100.0 μL fresh DMEM medium containing different concentrations of this biomass-based CDs at 0 (control), 0.01, 0.02, 0.05, 0.1, 0.2, 0.3, 0.5, 1.0, and 2.0 mg/mL for incubation at 37.0 °C, respectively. After 24.0 h, 50.0 μL, 1.0 mg/mL of MTT reagent was added into each well to carry out another 4.0 h incubation at 37.0 °C. Subsequently, the medium in each well was removed and further added with 150.0 μL DMSO. After 20.0 min shaking, the absorbance values at 490 nm of all wells were captured to assess the cell viability with the absorbance ratio before and after treatment with this biomass-based CDs. The involve all data were repeated three times at least.

3. Results and discussions

3.1. Synthesis and characterization of the biomass-based CDs

TEM image illustrated that the GSH assisting waste tobacco leaf-derived biomass-based CDs displayed a good monodispersity (Fig. 1A), with an average diameter of about 3.4 nm (Fig. 1B). Moreover, the high-resolution TEM (HRTEM) image showed the clear lattice stripes with 0.22 nm spacing, corresponding to the (100) face of graphite (inset of Fig. 1A).

Meanwhile, this biomass-based CDs exhibited a clear XRD diffraction peak at $2\theta = 21.3°$, assigning to the (002) face of the graphite crystal type (Fig. S1A). By profiling the Raman spectrum, this biomass-based CDs showed two characterize peaks at ~ 1340 and 1590 cm^{-1} (Fig. S1B). The former absorbance was primarily attributed to the disordered D-band of sp^3 defects, while the latter was resulting from the crystalline G-band of the in-plane vibrations of sp^2 carbon. These results clearly implied that this biomass-based CDs was a graphite-like structure. Next, the elemental composition of this biomass-based CDs was investigated by XPS analysis. From the full scan XPS spectrum, this biomass-based CDs could be mainly composed of C (285.1 eV), N (400.8 eV), O (531.4 eV), and S (163.9 eV) elements, respectively (Fig. 2 A). Therefore, the four peaks of 285.3, 286.1, 287.2, and 288.4 eV in the high-resolution C 1 s spectrum were probably attributed

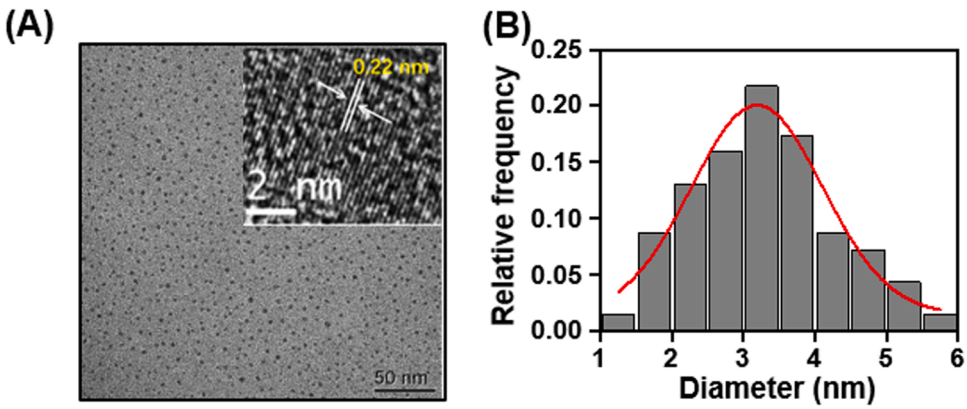

Fig. 1. (A) TEM image (inset: HRTEM image) and (B) particle size distribution of this biomass-based CDs.

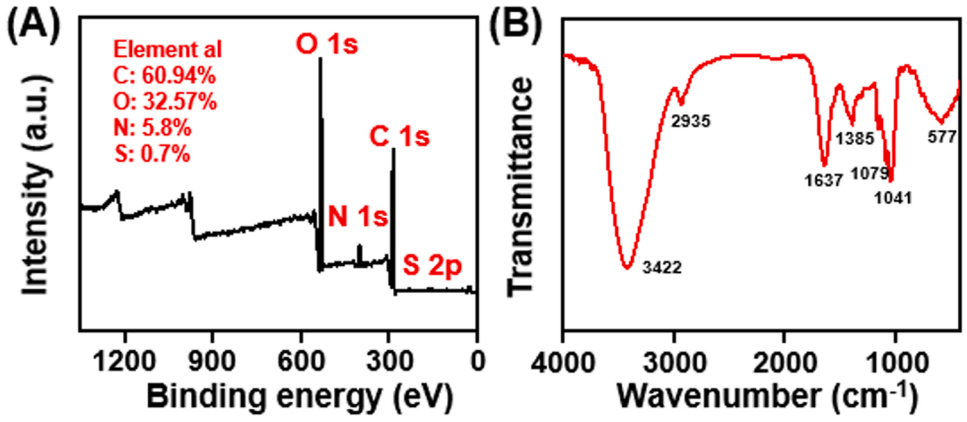

Fig. 2. (A) XPS spectrum and (B) FTIR spectrum of this biomass-based CDs.

to C-S, C-C/C-N, C–O, and C═O/C═N/C═S bonds, respectively (Fig. S2A) [37,38]. Likewise, two peaks of 533.7 eV and 534.9 eV in the high-resolution O 1 s spectrum indicated the existence C═O and C–OH/C–O–C bonds (Fig. S2B) [39]. Besides, the high-resolution N 1 s spectrum of this biomass-based CDs (Fig. S2C) showed that there were three peaks at 400.3, 401.0, and 401.7 eV, probably ascribable to the nitrogen species in the forms of C═N, N–C, and N–H, respectively [40, 41]. To further profile the high-resolution S 2p spectrum, two peaks at 163.8 and 164.7 eV indicated the S $2p_{3/2}$, S $2p_{1/2}$, and the existence of C-S bond on this biomass-based CDs (Fig. S2D). In combination with the FT-IR analysis (Fig. 2B), the absorption band at 3422 cm^{-1} proved the O–H and N–H stretching vibration, indicating the presence of $–NH_2$ and –OH groups on the surface of this biomass-based CDs [40,41]. The absorption band at 2935 cm^{-1} was resulting from the symmetric stretching vibration of the aliphatic C-H bond. The absorption band at 1637 and 1385 cm^{-1} could be identified as the symmetric and asymmetric stretching vibration of the C═O, C–N/N–H/COO^-, and C–O–C/C–O group, respectively. Notably, the absorption bands at 1079 and 1040 cm^{-1} belonged to the C-S and oxidized S bonds [18]. Based on these aforementioned results, there were abundant $–NH_2$, –COOH, –OH and C-S groups on the surface of this biomass-based CDs, endowing it good hydrophilicity and easy surface modification.

Having confirmed the successful synthesis of this GSH assisting waste tobacco leaf-derived biomass-based CDs, its optical properties were then

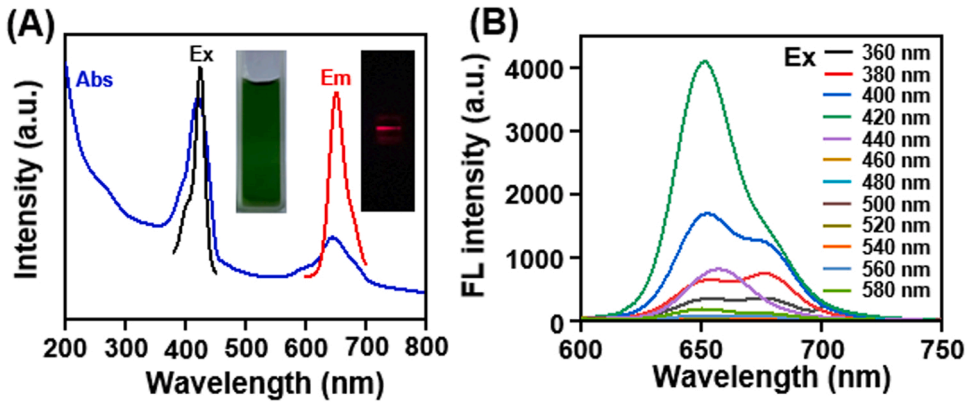

Fig. 3. (A) UV–vis absorption (blue), excitation (black) and emission (red) spectra of this biomass-based CDs; (B) Emission-dependent properties of this biomass-based CDs.

examined. As discovered in Fig. 3 A, this biomass-based CDs aqueous solution showed obvious green colour, with two characteristic absorption peaks at 420 and 652 nm, assigning to the n-π * electron transitions of the C═O bond [18,42]. As shown in Fig. 3B, when the excitation wavelength changed, the fluorescence emission peak shape and the intensity changed as well, indicating the excitation-dependent properties of this biomass-based CDs, which could be related to its surface oxidation degree. By fixing the maximum excitation wavelength at 420 nm, this biomass-based CDs showed a red fluorescence emission at 652 nm, with a bright red fluorescence colour in aqueous solution upon a 420 nm light excitation. Of particular mention was that this biomass-based CDs possessed a remarkable Stokes shift (232 nm) emission, which could be beneficial to avoid the overlap between excitation and emission, and to improve the detection sensitivity. We obtained this biomass-based CDs with a quantum yield of 11.04%. Moreover, the fluorescence emission of this biomass-based CDs aqueous solution remained stable in different pH, high ionic strength and under more than 100.0 min irradiation time (Fig. S3 & S4), implying excellent stability of this biomass-based CDs in aqueous solution.

3.2. Fluorescence assay of this biomass-based CDs toward Hg^{2+}

Encouraged by theses satisfactory features of this biomass-based in aforementioned aqueous solution, we then evaluated its selective fluorescence response ability for Hg^{2+} over other metal ions (e.g., Al^{3+}, Ba^{2+}, Ca^{2+}, Cd^{2+}, Co^{2+}, Cu^{2+}, Fe^{3+}, Mg^{2+}, Mn^{2+}, Ni^{2+}, Zn^{2+}, V^{3+}, V^{2+}, Sr^{2+}, Sn^{2+}, Pt^{4+}, Pd^{2+}, Pb^{2+}, Ag^{+}, and Hg^{2+}) in aqueous solution. The corresponding results showed that only Hg^{2+} could quench the fluorescence of this biomass-based CDs, while there was no significant effect of other metal ions on that of this biomass-based CDs in the same conditions. Which suggests a high selectivity of this biomass-based CDs for Hg^{2+} and thereby implying the feasibility of Hg^{2+} monitoring (Fig. 4A). To further verify its suitability in actual environmental media, the interference experiments were carried out. As shown in Fig. 4B, only Sn^{2+} had a weak effect on the Hg^{2+}-triggered CDs fluorescence quenching, indicating that this biomass-based CDs exhibited a remarkably high selectivity and potential for Hg^{2+} monitoring in real environment media. This might result from the strong interaction of Hg^{2+} toward the surface functional groups of this biomass-based CDs.

Driven by this, four important factors of this biomass-based CDs responding to Hg^{2+} were optimized, including pH, CDs concentration, incubation time and temperature. As illustrated in Fig. 5A, there was insignificant pH effect on the Hg^{2+}-trigged the fluorescence quenching efficiency ($1\text{-}F/F_0$) of this biomass-based CDs among the pH value ranging from 2.0 to 12.0. Meanwhile, it could be seen from the Fig. 5B that the maximum Hg^{2+}-trigged fluorescence quenching efficiency appeared at the 12.5 μg/mL of this biomass-based CDs. Similarly, as displayed in Fig. 5C & D, the maximum Hg^{2+}-trigged fluorescence quenching efficiency for this biomass-based CDs appeared at 20.0 ℃ after 30.0 min reaction.

Having explored the optimal experimental conditions, we continued to examine the analytical sensitivity of this biomass-based CDs for Hg^{2+} in B-R buffer. As described in Fig. 6A & B, under the optimal experimental conditions, there was a Hg^{2+} concentration-dependent fluorescence quenching of this biomass-based CDs at 652 nm in the range from 0.0 to 100.0 μM. By plotting the fluorescence quenching efficiency versus Hg^{2+} concentration, a calibration curve was populated with a linear expression of $(1\text{-}F/F_0) = 0.05107\ C + 0.08143$ (correlation coefficient $R^2 = 0.9994$) in the range from 0.09 to 16.25 μM (Inset of Fig. 6B). The corresponding detection limit (3σ/slope) of this biomass-based CDs toward Hg^{2+} was determined as 0.4474 μM.

Comparing with other reported fluorescence assay (Table 1), the detection limit of this biomass-based CDs for Hg^{2+} was comparable or even lower.

3.3. Monitoring Hg^{2+} in actual samples

To evaluate the feasibility of this biomass-based CDs for Hg^{2+} monitoring in actual samples, this biomass-based CDs were applied to monitor Hg^{2+} in environmental lake and tap water. Since no residues of Hg^{2+} were detected in these samples, spike and recovery experiments were performed. A series of different concentrations (i.e., 4.00, 8.00, & 10.00 μM) of Hg^{2+} were added to these samples for quantitative analysis with this proposed biomass-based CDs. As listed in Table 2, the recovery of this biomass-based CDs for Hg^{2+} monitoring in the range from 92.07 % to 102.00 % indicated a good accuracy of this biomass-based CDs for Hg^{2+} assay. Moreover, the relative standard deviations (R.S.D.) among the range of 1.05 % – 3.80 % suggested that this biomass-based CDs exhibited a good repeatability for Hg^{2+} detection in real environmental water samples. More significantly, these results of this biomass-based CDs for Hg^{2+} monitoring in actual water samples almost aligned with that of the detection results with ICP-AES. All these results strongly illustrated that this biomass-based CDs could be highly applicable for the precise detection of Hg^{2+} in actual environmental samples. Which showed an excellent potential for applications in environmental pollution traceability analysis with simple, rapid, economic, and eco-friendly merits.

3.4. Interaction mechanism of this biomass-based CDs with Hg^{2+}

Having illustrated the good fluorescence response of this biomass-based CDs toward Hg^{2+} in aqueous solution, the interaction mechanism of this biomass-based CDs with Hg^{2+} was subsequently examined. As the most intuitive technique for exploring the interaction information, the absorption spectra of this biomass-based CDs before and after incubation with Hg^{2+} were studied. As discovered in Fig. 7A, the

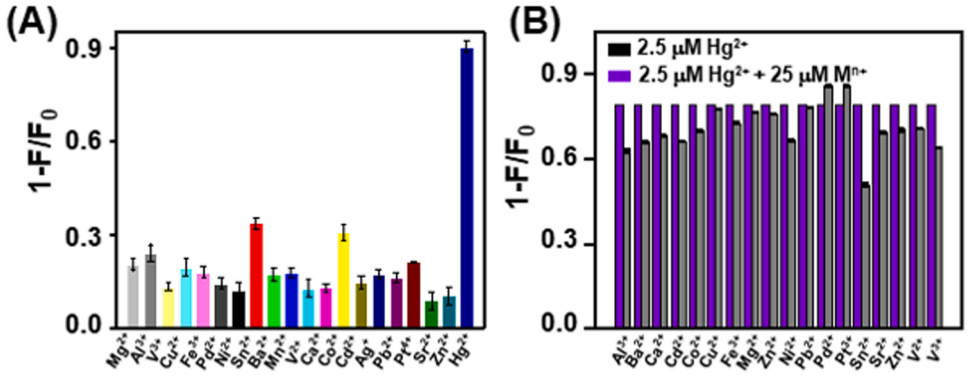

Fig. 4. (A) Selectivity of CDs for the detection of Hg^{2+} ([CDs] =12.5 μg/mL, [M^{n+}] =25 μM). (B) The effects of interfering metal ions on the detection of Hg^{2+} using CDs. [CDs] = 12.5 μg/mL, reaction in B-R buffer (pH 6.8) for 30.0 min at room temperature.

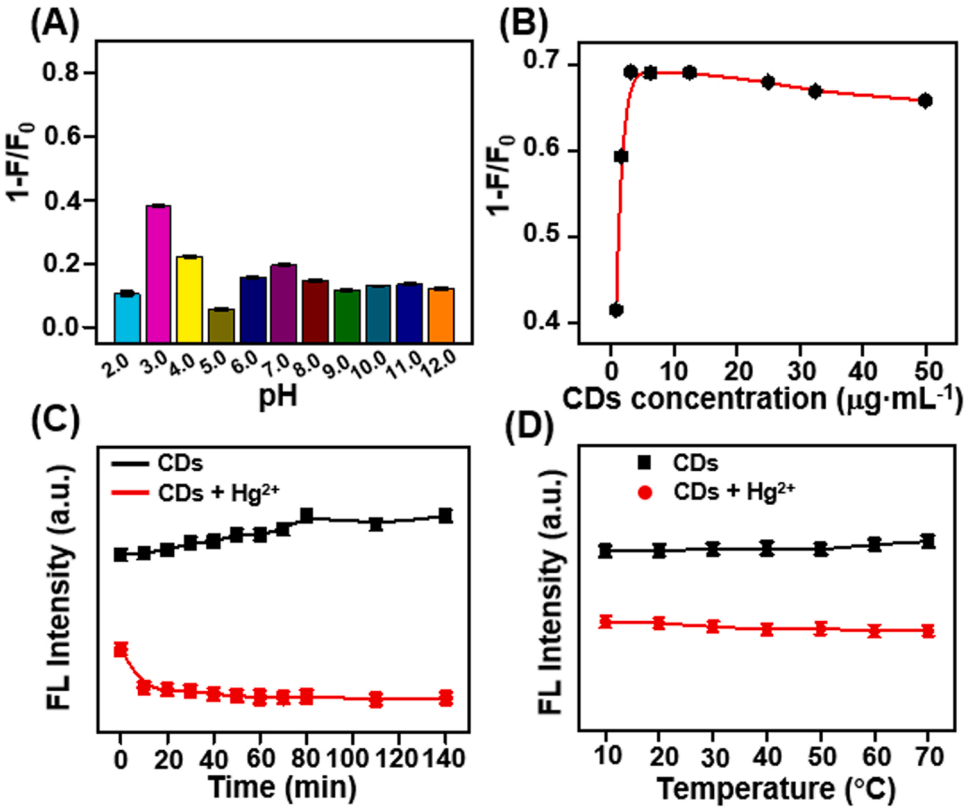

Fig. 5. Effect of pH (A), CDs concentration (B), reaction time (C), and temperature (D) on the FL quenching efficiency of Hg^{2+} towards CDs in B-R buffer (pH 6.8). [CDs] = 12.5 μg/mL, [Hg^{2+}] = 2.5 μM.

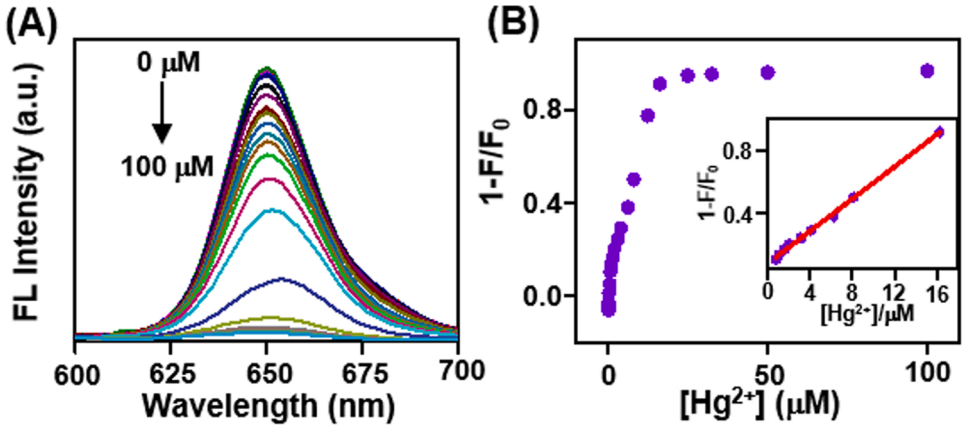

Fig. 6. (A) Fluorescence spectra of CDs before and after the addition of Hg^{2+} with various concentrations. (B) Plot of 1-F/F_0 versus [Hg^{2+}]. Inset: liner relationship of 1-F/F_0 vs [Hg^{2+}] in the range of 0.09 16.25 μM (n = 3).

introduced Hg^{2+} could cause the intensity decrease in the absorption peaks of this biomass-based CDs both at 420 and 652 nm, accompanied by obvious red-shift of these two absorption peaks, suggesting a strong binding of CDs with Hg^{2+} for resulting in the increase of CDs surface polarity as well as its size (Table S1) [49]. As exhibited in Fig. 7B, through fluorescence lifetime measurements, the negligible lifetime changed of CDs before (3.7814 ns) and after (3.7228 ns) incubation with Hg^{2+} excluded the fluorescence resonance energy transfer behavior in the fluorescence response of this biomass-based CDs toward Hg^{2+}. In this case, as shown in Fig. 7C, by performing centrifugation, there was an obvious separated layer, i.e., the supernatant was almost colorless, while a large amount of precipitation appeared in the sublayer, indicating that Hg^{2+} could induce the aggregation of this biomass-based CDs to further cause its fluorescence quenching via the aggregation-caused quenching (ACQ) mechanism.

From the XPS and FT-IR characterization results above, there were abundant –NH_2, –COOH, –OH, and C-S groups on the surface of this biomass-based CDs, which have been confirmed to display high coordination abilities with metal ions [50-52]. To confirm these points, we then explored the roles of these functional groups in Hg^{2+}-triggered aggregation behavior of this biomass-based CDs. These functional groups were protected respectively based on surface chemistry strategy, and the protection was confirmed to be successful by FTIR and ^{1}HNMR (Fig. S5). Considering the weak binding constants of sodium 1,3-propane sulfonate (PS) to metal ions, PS was chosen experimentally as the passivating reagent to protect –NH_2, –COOH, and –OH groups on this

Table 1
Comparison of the prepared biomass-based CDs with other materials for detecting and removing Hg^{2+}.

Probe	Method	Linear range (μM)	Detection limit (μM)	Removal efficiency (%)	Ref
Carbon dots	Fluorescence	0.01 – 2.50	3.6×10^{-3}	N.M.	[43]
Carbon dots	Fluorescence	0 – 400	0.9	N.M.	[44]
N-Carbon dots	Fluorescence	0.1 – 5.0	0.019	N.M.	[45]
B/N-Carbon dots	Fluorescence	5 – 175	2.8	N.M.	[46]
Carbon dots	Fluorescence	1.18 – 47	0.67	N.M.	(Yang, Cui et al. 2020)
Polymeric Probe	Fluorescence	1×10^{-3} – 1.0	1.5×10^{-3}	94	[47]
Polymeric Nanospheres	Fluorescence	0 – 200	0.012	99.9	[48]
CDs	Fluorescence	0.09 – 16.25	0.4474	99.4	our work

N.M. means "not mentioned".

Table 2
Detecting of Hg^{2+} using this biomass-based CDs in lake and tap water by the standard addition method.

Sample	Added/ (μM)	Found / (μM)	Recovery / (%)	R.S.D. / (n = 3, %)	ICP-AES / (μM)
Lake water	4.000	4.080	102.0	3.800	3.832
	8.000	7.890	98.62	3.410	7.916
	12.00	11.06	92.17	2.970	12.43
Tap water	4.000	3.840	96.00	1.050	3.862
	8.000	8.130	101.6	3.550	7.548
	12.00	11.75	97.92	2.800	12.32

biomass-based CDs, achieving the passive CDs was named as CDs-PS [53]. In this case, the Hg^{2+}-triggered fluorescence quenching behavior of CDs-PS still occurred, but was much lower than that free CDs (Fig. 8A), implying that other groups (NH_2, –COOH, and –OH groups) on the surface of this biomass-based CDs also played a significant role in Hg^{2+}-triggered its fluorescence quenching behavior. Despite this, the contribution of S-Hg bond to the CDs aggregation was only part, owing to the relatively low fluorescence quenching efficiency of Hg^{2+} toward the passive CDs-PS, implying that the other groups could also play a role in Hg^{2+}-induced CDs aggregation. Since esters were easily hydrolyzed to form original carboxylic acids under alkaline conditions but others not, CDs-PS was put into a NaOH solution in a water bath, and a sample protecting only $–NH_2$ and –OH groups were obtained, which was called as CDs-PS-NaOH [53]. Meanwhile, the 4-sulfophenyl isothiocyanate (SPI) was further chosen as a passive reagent to protect the $–NH_2$ group

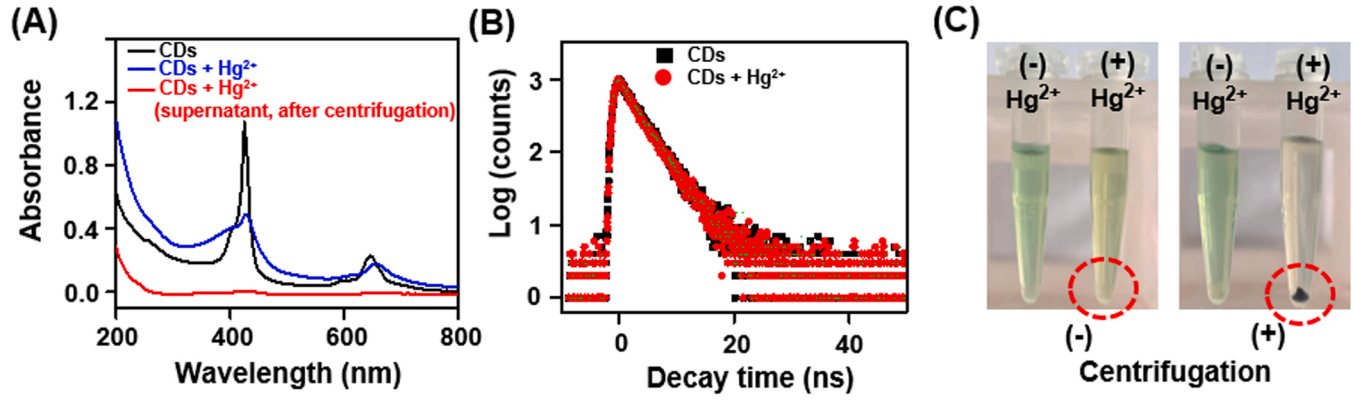

Fig. 7. UV–vis absorption spectra (A), fluorescence decay curves (B) and photographs (C) of CDs before and after interaction with Hg^{2+}. [CDs] = 100.0 μg/mL, [Hg^{2+}] = 100.0 μM, reaction in B-R buffer (pH 6.8) for 30.0 min at room temperature.

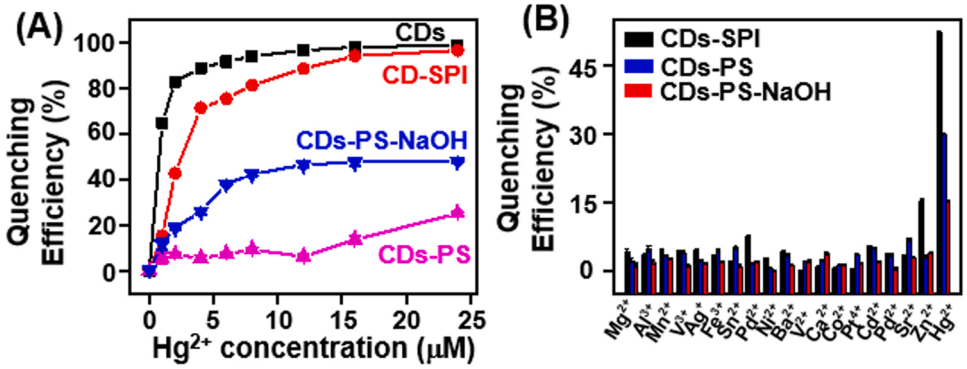

Fig. 8. (A) Quenching efficiency of CDs, CDs-SPI, CDs-PS, and CDs-PS-NaOH under different concentrations of Hg^{2+}. [CDs], [CDs-SPI], [CDs-PS], [CDs-PS-NaOH] are 100.0 μg/mL, Hg^{2+} concentration from 0.0 to 25.0 μM. (B) Selectivity of CDs-SPI, CDs-PS, and CDs-PS-NaOH towards Hg^{2+}. [CDs-SPI], [CDs-PS], and [CDs-PS-NaOH] are 12.5 μM, [M^{n+}] = 2.5 μM.

on this CDs, yielding the passive CDs was named as CDs-SPI [54,55]. On this occasion, we noticed that the Hg^{2+}-triggered quenching efficiency for CDs-PS-NaOH was lower than that for free CDs, but higher than that for CDs-PS. Apart from this, when the Hg^{2+} concentration was below 16.0 μM, the Hg^{2+}-triggered fluorescence quenching efficiency of CDs-SPI was lower than that of free CDs. These findings probably proved the significant role of –COOH, $–NH_2$ and –OH groups in the Hg^{2+}-triggered CDs aggregation. Additionally, as displayed in Fig. 8B, the fluorescence response of CDs-SPI, CDs-PS and CDs-PS-NaOH to the following metal ions were evaluated, including Mg^{2+}, Al^{3+}, Mn^{2+}, V^{3+}, Ag^{+}, Fe^{3+}, Sn^{2+}, Pd^{2+}, Ni^{2+}, Ba^{2+}, V^{2+}, Ca^{2+}, Co^{2+}, Pt^{4+}, Cd^{2+}, Pb^{2+}, Sr^{2+}, Zn^{2+}, and Hg^{2+}. The results showed that the modified CDs had no effect on the selectivity of metal ions and still maintained a high specificity for Hg^{2+}.

It has been reported that Hg^{2+} exhibited a relatively high affinity toward biothiols (e.g., L-Cys, GSH, or Hcy) via Hg-S bond, whose binding constant was ~10 orders of magnitude larger than those of other nucleophiles under the same conditions [6]. In combination with the existence of C-S groups on the surface of this biomass-based CDs, we speculated that S-Hg bond was contributable to the Hg^{2+}-induced CDs aggregation. To confirm this, the competition effects of biothiols on Hg^{2+}-triggered CDs fluorescence quenching were examined. As depicted in Fig. 9A to D, the typical biothiols such as Hcy, L-Cys, and GSH were capable of interfering and impairing the fluorescence quenching efficiency of this biomass-based CDs caused by Hg^{2+}, clearly revealing the formation of S-Hg bond on the surface of this biomass-based CDs to facilitate its aggregation. Based on this, this study also constructed a highly sensitive and selective "off – on" method for the detection of biothiols using this biomass CDs as a fluorescent probe (Fig. S6 & S7).

According to the primary analysis above, we could be convinced that Hg^{2+}-induced the aggregation of this biomass-based CDs was due to the synergistic Hg-S bond and the coordination effects of the Hg^{2+} to the abundant –COOH, $–NH_2$ and –OH groups on the surfaces of this biomass-based CDs.

3.5. Exploration of the Hg^{2+} removal

Having confirmed the Hg^{2+}-induced CDs aggregation, we next tried to examine the removal ability of this biomass-based CDs for Hg^{2+} in the polluted aqueous media. 100.0 μg/mL CDs was added into 100.0 μM Hg^{2+} aqueous solution for 30.0 min mixing. After incubation of CDs with Hg^{2+}, the color of this biomass-based CDs solution changed from green to yellow. With the assistance of centrifugation, there appeared precipitation. The Hg^{2+} content in the precipitation was measured with classical ICP-AES. The results showed that 0.5488 μM of detectable Hg^{2+} remained in the supernatant. In this case, the settling efficiency of Hg^{2+} in the precipitation reached to be ~ 99.4 %, implying that the removal efficiency of this biomass-based CDs for Hg^{2+} could reach to be ~ 99.4 %. As compared with other reported removal materials for Hg^{2+} (Table 1), this proposed biomass-based CDs displayed a comparable or even better removal ability for Hg^{2+}. Besides, the removal conditions of this biomass-based CDs for Hg^{2+} were optimized. The optimal reaction time and biomass-based CDs concentration were 30.0 min and 100.0 μg/mL. As shown in Fig. 10A, this proposed biomass-based CDs removed > 97.0 % of Hg^{2+} within 20.0 min. Meanwhile, the removal efficiency of this biomass-based CDs for Hg^{2+} gradually increased with the increase of this biomass-based CDs concentration, and the removal efficiency was > 99 % at the concentration of this biomass-based CDs at 100.0 μg/mL (Fig. 10B). Notably, the influences of the co-existed metal ions (e.g., Al^{3+}, Fe^{3+}, Cr^{3+}, Cu^{2+}, Mg^{2+}, Pb^{2+}, Co^{2+}, Ni^{2+}, Cd^{2+}, & Ca^{2+}) on the removal efficiency of this biomass-based CDs for Hg^{2+} remained above 94.0% within 30.0 min (Fig. 10C).

To reveal the practicability of this biomass-based CDs for Hg^{2+} removal, it was used to remove Hg^{2+} from the spiked pond water. As shown in Fig. 11A & B, the amount of Hg^{2+} could be reduced to 7.37, 7.09, 8.94 and 24.55 μM by precipitation removal treatment at the standard levels of 60.0, 80.0, 100.0, and 200.0 μM. The removal efficiencies were 87.72 %, 91.13 % 91.06 %, and 90.18 %, respectively.

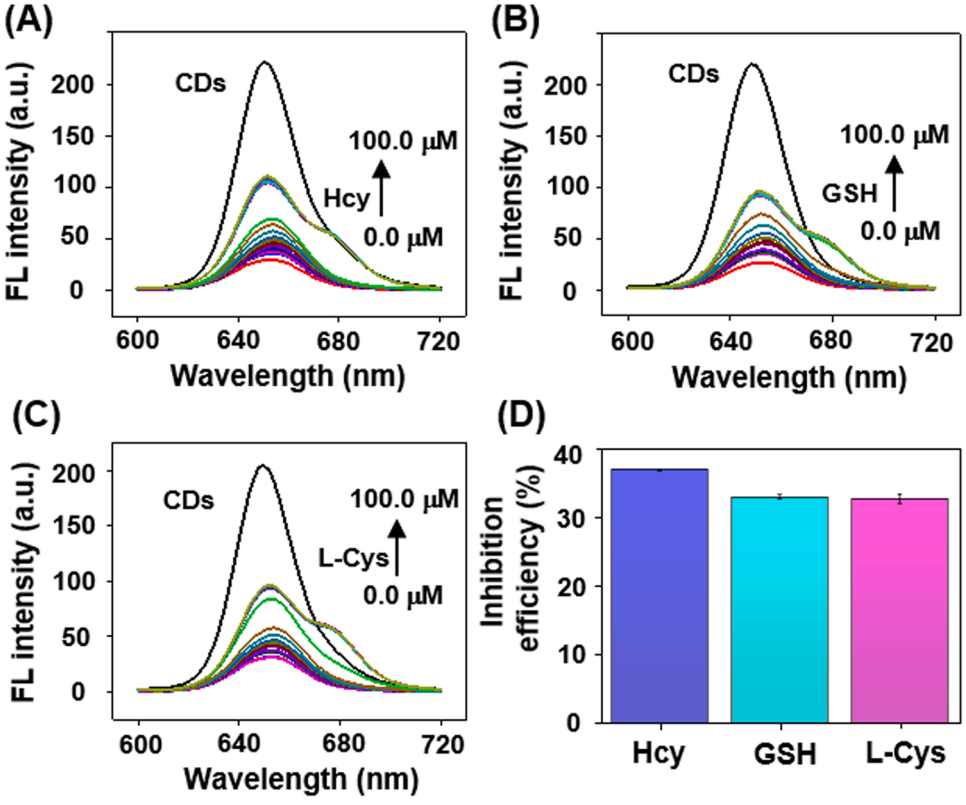

Fig. 9. FL response of CDs-Hg^{2+} system to Hcy (A), GSH (B), and L-Cys (C) with different concentrations. [CDs] = 12.5 μg/mL, [Hg^{2+}] = 2.5 μM, [Hcy], [GSH], and [L-Cys] concentration from 0.0 – 100.0 μM; (D) The inhibition of the quenching efficiency of Hcy, GSH and L-Cys to CDs-Hg^{2+} system.

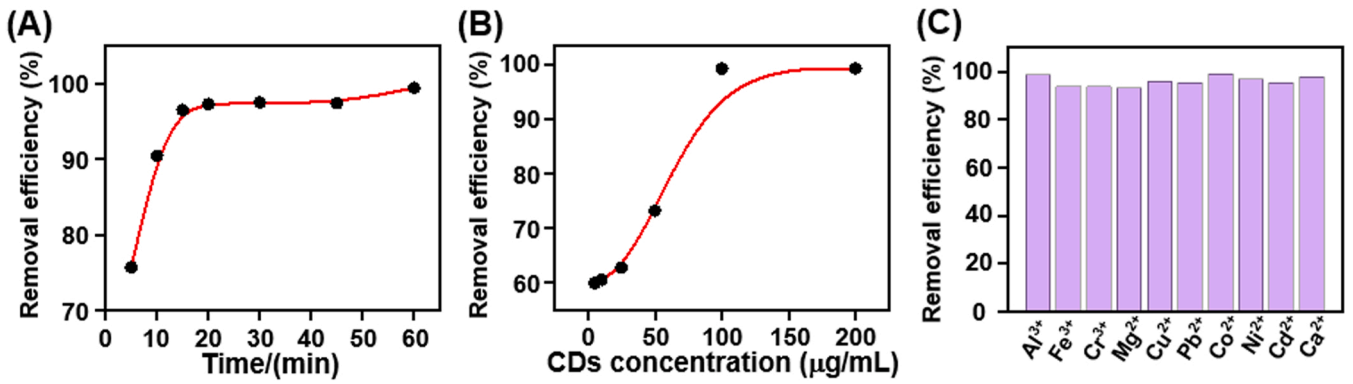

Fig. 10. Effect of reaction time (A), CDs concentration (B), and possible interfering metal ions (C) on the removal efficiency of CDs towards Hg^{2+}. [CDs] = 100.0 μg/mL, [Hg^{2+}] = 50.0 μM, [M^{n+}] = 70.0 μM, reaction in B-R buffer (pH 6.8) for 30.0 min at room temperature.

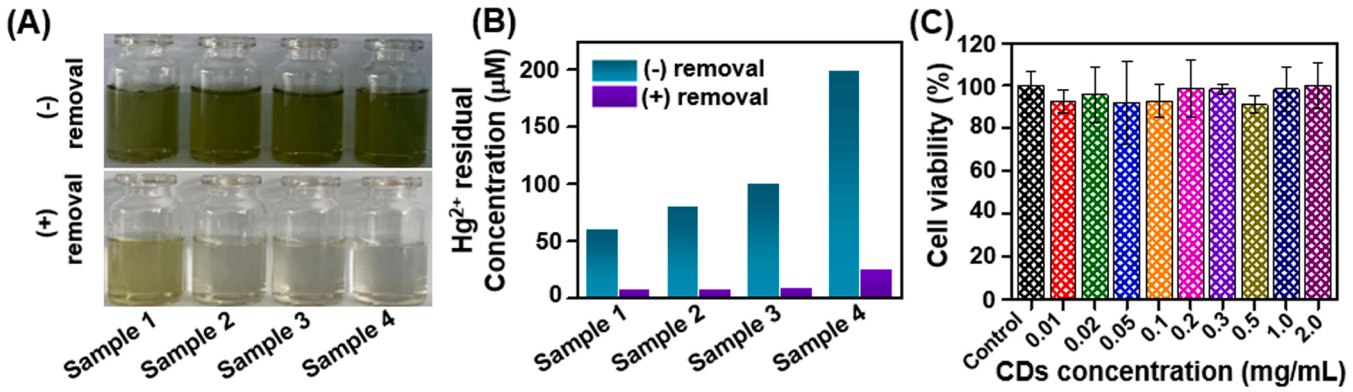

Fig. 11. (A) Application of this biomass-based CDs for Hg^{2+} removal from pond water. Sample 1–4 denotes the 60.0, 80.0, 100.0, 200.0 μM spike levels, respectively. [CDs] = 100.0 μg/mL, reaction for 30.0 min at room temperature. (B) Hg^{2+} removal ability of this biomass-based CDs at different spiked levels. (C) Cell viability for Hela cells in the presence of this biomass-based CDs with different concentrations (0.0, 0.01, 0.02, 0.05, 0.1, 0.2, 0.3, 0.5, 1.0, 2.0 mg/mL).

It is well-known that the environmental safety could be regarded as one of the important parameters to evaluate the popularization and application of the anti-fouling materials. Regarding this, we finally conducted the risk assessment of this biomass-based CDs toward the environmental safety through exploring its effect on the cell viability. We adopted the classic standard 3-(4,5-dimethylthiazol-2-yl)− 2,5-diphenyltetrazolium bromide (MTT) assay to evaluate the cytotoxicity of this biomass-based CDs on living human cervical carcinoma HeLa cells. As depicted in Fig. 11 C, after HeLa cell exposure toward this biomass-based CDs for over 24.0 h, the cell viability remained over 91.19%, even the concentration of this biomass-based CDs at 2.0 mg/mL, which was 20.0-fold higher than that applied in the test of Hg^{2+} removal, suggesting that this biomass-based CDs possessed a very low cytotoxicity. This fact strongly illustrated that this GSH assisting waste tobacco leaf-derived biomass-based CDs had a prominent biocompatibility to satisfy the eco-friendly demand in the application of removing Hg^{2+} from waste water.

4. Conclusions

In conclusion, a novel dual-functional biomass-based CDs derived from GSH assisting the waste tobacco leaf has been successfully synthesized for simultaneously precise fluorescence traceability and high-efficient removal of Hg^{2+} pollution in environmental matrices. Through optical analysis, this biomass-based CDs possessed a red fluorescence emission at ~ 652 nm with a remarkable Stokes shift of ~ 232 nm, which was beneficial to reduce/avoid the background signal interference for developing a reliable and highly sensitive fluorescence assay for Hg^{2+} monitoring in real environmental water samples with a low LOD of 0.45 μM. By profiling the response mechanism, Hg^{2+} could selectively trigger the aggregation of this biomass-based CDs via the synergistic Hg-S bond and the coordination effects of the Hg^{2+} to the abundant –COOH, –NH_2 and –OH groups on the surfaces of this biomass-based CDs, ultimately resulting in the fluorescence quenching of this biomass-based CDs via ACQ mechanism. Additionally, this Hg^{2+}-triggered aggregation behavior could facilitate the effective embedding and encapsulation of Hg^{2+} by into the aggregated CDs, which could yield the separation of Hg^{2+} for further removal with a high efficiency of 99.4% in wastewater in a rapid, simple, low-cost, and eco-friendly way. This work not only exhibited the novel insight into recycling the waste tobacco leaf for sustainable development, but also revealed the great potential of its derived biomass-based CDs for simultaneous monitoring and removal of Hg^{2+} in wastewater, which could be of great significance for both fundamental studies and practical applications.

CRediT authorship contribution statement

Hui Yang and Xiankun Su contributed equally to this work. **Hui Yang:** Conceptualization, Investigation, Data curation, Writing – original draft. **Xiankun Su:** Writing – review & editing, Funding acquisition. **Li Cai:** Investigation. **Zhenchun Sun:** Formal analysis. **Yechun Lin:** Writing – review & editing. **Jing Yu:** Formal analysis. **Likai Hao:** Supervision, Writing – review & editing. **Cui Liu**: Conceptualization, Methodology, Supervision, Writing – review & editing.

Declaration of Competing Interest

The authors declare that they have no known competing financial

interests or personal relationships that could have appeared to influence the work reported in this paper.

Data Availability

No data was used for the research described in the article.

Acknowledgments

This work was supported by the Science and Technology Project of Guizhou Company of China Tobacco Corporation (2022XM16), the Science and Technology Project of Guizhou Academy of Tobacco Science (GZYKY2021-07) and the Guizhou Provincial Science and Technology Department funded project ([2020]4102), the Guizhou Province Technology R&D Program ([2019]2398), the National Natural Science Foundation of China (41877400), and the Fundamental Research Funds for the Central Universities of China (JZ2021HGTB0113).

Appendix A. Supporting information

Supplementary data associated with this article can be found in the online version at doi:10.1016/j.jece.2022.108718.

References

[1] S. Ma, Q. Zhang, J. Zhu, H. Shi, K. Zhang, Y. Shen, Rational engineering of Ag-doped reduced graphene oxide as electrochemical sensor for trace mercury ions monitoring, Sens. Actuators B: Chem. 345 (2021), 130383.
[2] S. Rashid, I.A. Shah, R.X. Supe Tulcan, W. Rashid, M. Sillanpaa, Contamination, exposure, and health risk assessment of Hg in Pakistan: a review, Environ. Pollut. 301 (2022), 118995.
[3] Y. Shen, Y. Wei, C. Zhu, J. Cao, D.-M. Han, Ratiometric fluorescent signals-driven smartphone-based portable sensors for onsite visual detection of food contaminants, Coord. Chem. Rev. 458 (2022), 214442.
[4] Y. Shen, C. Nie, Y. Wei, Z. Zheng, Z.-L. Xu, P. Xiang, FRET-based innovative assays for precise detection of the residual heavy metals in food and agriculture-related matrices, Coord. Chem. Rev. 469 (2022), 214676.
[5] G. Li, M. Lu, S. Li, M. Yang, Y. Zhang, Y. Zhang, H. Wang, W. Yang, A novel fluorescent "OFF-ON" sensing strategy for Hg (II) in water based on functionalized gold nanoparticles, Chemosphere 303 (2022), 135174.
[6] K. Zhang, G. Zhu, Y. Wei, L. Zhang, Y. Shen, Engineering of an upconversion luminescence sensing platform based on the competition effect for mercury-ion monitoring in green tea, J. Agric. Food Chem. 69 (30) (2021) 8565–8570.
[7] N.D. Rudd, H. Wang, E.M.A. Fuentes-Fernandez, S.J. Teat, F. Chen, G. Hall, Y. J. Chabal, J. Li, Highly efficient luminescent metal–organic framework for the simultaneous detection and removal of heavy metals from Water, ACS Appl. Mater. Interfaces 8 (44) (2016) 30294–30303.
[8] X. Wang, C. Hu, X. Wang, Z. Luo, S. Zhen, L. Zhan, C. Huang, Y. Li, Facile synthesis of dual-ligand terbium-organic gels as ratiometric fluorescence probes for efficient mercury detection, J. Hazard. Mater. 436 (2022), 129080.
[9] J. Li, S. Wang, X. Cao, H. Huang, D. Cao, Sulfur-modified porous covalent organic polymers as bifunctional materials for efficient fluorescence detection and fast removal of heavy metal ions, Mater. Chem. Front. 5 (8) (2021) 3428–3435.
[10] Q. Sun, B. Aguila, J. Perman, L.D. Earl, C.W. Abney, Y. Cheng, H. Wei, N. Nguyen, L. Wojtas, S. Ma, Postsynthetically modified covalent organic frameworks for efficient and effective mercury removal, J. Am. Chem. Soc. 139 (7) (2017) 2786–2793.
[11] C. Long, X. Li, Z. Jiang, P. Zhang, Z. Qing, T. Qing, B. Feng, Adsorption-improved $MoSe_2$ nanosheet by heteroatom doping and its application for simultaneous detection and removal of mercury (II), J. Hazard. Mater. 413 (2021), 125470.
[12] Y.Y. Wang, M.Y. Tang, H. Shen, G.B. Che, Y. Qiao, B. Liu, L. Wang, Recyclable multifunctional magnetic mesoporous silica nanocomposite for ratiometric detection, rapid adsorption, and efficient removal of Hg(II), ACS Sustain. Chem. Eng. 6 (2) (2018) 1744–1752.
[13] Y.Z. Fan, L. Han, Y.Z. Yang, Z. Sun, N. Li, B.L. Li, H.Q. Luo, N.B. Li, Multifunctional binding strategy on nonconjugated polymer nanoparticles for ratiometric detection and effective removal of mercury ions, Environ. Sci. Technol. 54 (16) (2020) 10270–10278.
[14] L. Feng, W.-M. Chen, J.-L. Li, G. Day, H. Drake, E. Joseph, H.-C. Zhou, Biological antagonism inspired detoxification: removal of toxic elements by porous polymer networks, ACS Appl. Mater. Interfaces 11 (15) (2019) 14383–14390.
[15] L. Chen, Q. Wu, J. Gao, H. Li, S. Dong, X. Shi, L. Zhao, Applications of covalent organic frameworks in analytical chemistry, TrAC Trends Anal. Chem. 113 (2019) 182–193.
[16] H. Musarurwa, L. Chimuka, N.T. Tavengwa, Sorptive extraction of pesticides from food and environmental samples using metal organic framework-based adsorbents, Trends Environ. Anal. Chem. 32 (2021), e00141.
[17] Y. Wang, M. Zhang, X. Shen, H. Wang, H. Wang, K. Xia, Z. Yin, Y. Zhang, Biomass-derived carbon materials: controllable preparation and versatile applications, Small 17 (40) (2021).
[18] M. Zhou, Z. Zhou, A. Gong, Y. Zhang, Q. Li, Synthesis of highly photoluminescent carbon dots via citric acid and tris for iron (III) ions sensors and bioimaging, Talanta 143 (2015) 107–113.
[19] B. Wang, H. Cai, G.I. Waterhouse, et al., Carbon dots in bioimaging, biosensing and therapeutics: a comprehensive review small, Science 2200012 (2022).
[20] S. Bilge, L. Karadurmus, A. Sinag, S.A. Ozkan, Green synthesis and characterization of carbon-based materials for sensitive detection of heavy metal ions, Trac-Trends Anal. Chem. 145 (2021), 116473.
[21] V. Manikandan, N.Y. Lee, Green synthesis of carbon quantum dots and their environmental applications, Environ. Res. 212, Part B (2022), 113283.
[22] S. Ren, B. Liu, M. Wang, G. Han, H. Zhao, Y. Zhang, Highly bright carbon quantum dots for flexible anti-counterfeiting, J. Mater. Chem. C 10 (31) (2022) 11338–11346.
[23] X. Wang, Y. Zhang, J. Li, G. Liu, M. Gao, S. Ren, B. Liu, L. Zhang, G.T. Han, J.Y. Yu, H.G. Zhao, F. Rosei, Platinum cluster/carbon quantum dots derived graphene heterostructured carbon nanofibers for efficient and durable solar-driven electrochemical hydrogen evolution, Small Methods 6 (2022), 2101470.
[24] K. Qi, Y. Ye, B. Wei, M. Li, Y. Lun, X. Xie, H. Xie, N-CQDs from reed straw enriching charge over BiO_2-x/$BiOCl_{p-n}$ heterojunction for improved visible-light-driven photodegradation of organic pollutants, J. Hazard. Mater. 432 (2022), 128759.
[25] A. Raza, S. Altaf, S. Ali, M. Ikram, G. Li, Recent advances in carbonaceous sustainable nanomaterials for wastewater treatments, Sustain. Mater. Technol. 32 (2022), e0046.
[26] F. Shan, L. Fu, X. Chen, X. Xie, C. Liao, Y. Zhu, H. Xia, J. Zhang, L. Yan, Z. Wang, X. Yu, Waste-to-wealth: Functional biomass carbon dots based on bee pollen waste and application, Chin. Chem. Lett. 33 (6) (2022) 2942–2948.
[27] H. Yang, Y. Wei, X. Yan, C. Nie, Z. Sun, L. Hao, X. Su, High-efficiency utilization of waste tobacco stems to synthesize novel biomass-based carbon dots for precise detection of tetracycline antibiotic residues, Nanomaterials 12 (2022) 3241.
[28] H. Liu, L. Ding, L. Chen, Y. Chen, T. Zhou, H. Li, Y. Xu, L. Zhao, N. Huang, A facile, green synthesis of biomass carbon dots coupled with molecularly imprinted polymers for highly selective detection of oxytetracycline, J. Ind. Eng. Chem. 69 (2019) 455–463.
[29] G. Chellasamy, S.K. Arumugasamy, S. Govindaraju, K. Yun, Green synthesized carbon quantum dots from maple tree leaves for biosensing of Cesium and electrocatalytic oxidation of glycerol, Chemosphere 287 (2022), 131915.
[30] P.K. Yadav, V.K. Singh, S. Chandra, D. Bano, V. Kumar, M. Talat, S.H. Hasan, Green synthesis of fluorescent carbon quantum dots from Azadirachta indica leaves and their peroxidase-mimetic activity for the detection of H_2O_2 and ascorbic acid in common fresh fruits, ACS Biomater. Sci. Eng. 5 (2) (2019) 623–632.
[31] P. Krishnaiah, R. Atchudan, S. Perumal, E.-S. Salama, Y.R. Lee, B.-H. Jeon, Utilization of waste biomass of Poa pratensis for green synthesis of N-doped carbon dots and its application in detection of Mn^{2+} and Fe^{3+}, Chemosphere 286 (2022), 131764.
[32] Z. Li, Q. Wang, Z. Zhou, S. Zhao, S. Zhong, L. Xu, Y. Gao, X. Cui, Green synthesis of carbon quantum dots from corn stalk shell by hydrothermal approach in near-critical water and applications in detecting and bioimaging, Microchem. J. 166 (2021), 106250.
[33] Y. Wang, Q. He, X. Zhao, J. Yuan, H. Zhao, G. Wang, M. Li, Synthesis of corn straw-based graphene quantum dots (GQDs) and their application in PO_4^{3-} detection, J. Environ. Chem. Eng. 10 (2) (2022), 107150.
[34] M. Xue, Z. Zhan, M. Zou, L. Zhang, S. Zhao, Green synthesis of stable and biocompatible fluorescent carbon dots from peanut shells for multicolor living cell imaging, New J. Chem. 40 (2) (2016) 1698–1703.
[35] H. Fujioka, S.-n Uno, M. Kamiya, R. Kojima, K. Johnsson, Y. Urano, Activatable fluorescent probes for hydrolase enzymes based on coumarin-hemicyanine hybrid fluorophores with large Stokes shifts, Chem. Commun. 56 (42) (2020) 5617–5620.
[36] X. Xiao, W. Tingting, C. Jinxuan, Z. Chunlei, L. Yuan, Z. Xin, S. Yizhong, Rational engineering of chromic material as near-infrared ratiometric fluorescent nanosensor for H_2S monitoring in real food samples, Sens. Actuators B: Chem. 323 (2020), 128707.
[37] Y. Hu, J. Yang, J. Tian, L. Jia, J.-S. Yu, Waste frying oil as a precursor for one-step synthesis of sulfur-doped carbon dots with pH-sensitive photoluminescence, Carbon 77 (2014) 775–782.
[38] Atchudan Raji, Nesakumar Thomas, Immanuel Jebakumar, Kanikkai Edison, Raja, Aseer, Highly fluorescent nitrogen-doped carbon dots derived from Phyllanthus acidus utilized as a fluorescent probe for label-free selective detection of Fe^{3+} ions, live cell imaging and fluorescent ink, Biosens. Bioelectron. 99 (2018) 303–311.
[39] Q. Su, X. Wei, J. Mao, X. Yang, Carbon nanopowder directed synthesis of carbon dots for sensing multiple targets, Colloids Surf. A: Physicochem. Eng. Asp. 562 (2018) 86–92.
[40] W. Lu, Y. Jiao, Y. Gao, J. Qiao, M. Mozneb, S. Shuang, C. Dong, C.Z. Li, bright yellow fluorescent carbon dots as a multifunctional sensing platform for the label-free detection of fluoroquinolones and histidine, ACS Appl. Mater. Interfaces 10 (49) (2018) 42915–42924.
[41] Y. Yan, J.H. Liu, R.S. Li, Y.F. Li, C.Z. Huang, S.J. Zhen, Carbon dots synthesized at room temperature for detection of tetracycline hydrochloride, Anal. Chim. Acta 1063 (2019) 144–151.
[42] C. Shen, Y. Sun, J. Wang, Y. Lu, Facile route to highly photoluminescent carbon nanodots for ion detection, pH sensors and bioimaging, Nanoscale 6 (15) (2014) 9139–9147.

[43] Q. Zhou, L. Yongli, Y. Wu, Z. Li, Y. Li, M. Liu, T. Qu, C. Chen, Measurement of mercury with highly selective fluorescent chemoprobe by carbon dots and silver nanoparticles, Chemosphere 274 (2021), 129959.
[44] X. Hao, S. Dai, J. Wang, Z. Fang, Synthesis of blue fluorescent carbon dots and their application in detecting mercury and iodine based on "off–on" mode, Luminescence 36 (3) (2021) 721–732.
[45] S. Liao, X. Li, H. Yang, X. Chen, Nitrogen-doped carbon dots rapid and selective detection of mercury ion and biothiol and construction of an IMPLICATION logic gate, Talanta 194 (2019) 554–562.
[46] L.-F. Pang, H. Wu, M.-J. Fu, X.-F. Guo, H. Wang, Red emissive boron and nitrogen co-doped "on-off-on" carbon dots for detecting and imaging of mercury(II) and biothiols, Microchim. Acta 186 (11) (2019) 708.
[47] N. Choudhury, B. Saha, B. Ruidas, P. De, Dual-action polymeric probe: Turn-On sensing and removal of Hg^{2+}; Chemosensor for HSO_4^-, ACS Appl. Polym. Mater. 1 (461–471) (2019).
[48] Y. Fu, W. Yu, W. Zhang, Q. Huang, J. Yan, C. Pan, G. Yu, Sulfur-rich covalent triazine polymer nanospheres for environmental mercury removal and detection, Polym. Chem. 9 (30) (2018) 4125–4131.
[49] Y. Shen, T. Wu, Y. Zhang, N. Ling, L. Zheng, S.-L. Zhang, Y. Sun, X. Wang, Y. Ye, Engineering of a dual-recognition ratiometric fluorescent nanosensor with a remarkably large stokes shift for accurate tracking of pathogenic bacteria at the single-cell level, Anal. Chem. 92 (19) (2020) 13396–13404.
[50] Lakowicz, J. and Lakowicz, 2008. Principles of fluorescence spectroscopy, Principles of fluorescence spectroscopy.
[51] Z. Li, Y. Wang, Y. Ni, S. Kokot, A rapid and label-free dual detection of Hg (II) and cysteine with the use of fluorescence switching of graphene quantum dots, Sens. Actuators B: Chem. (2015) 490–497.
[52] J.M. Liu, L.P. Lin, X.X. Wang, S.Q. Lin, W.L. Cai, L.H. Zhang, Z.Y. Zheng, Highly selective and sensitive detection of Cu^{2+} with lysine enhancing bovine serum albumin modified-carbon dots fluorescent probe, Analyst 137 (11) (2012) 2637.
[53] M. Yang, C. Liu, Y. Peng, R.-Z. Xiao, S. Zhang, Z.-L. Zhang, B. Zhang, D.-W. Pang, Surface chemistry tuning the selectivity of carbon nanodots towards Hg^{2+} recognition, Anal. Chim. Acta 1146 (2021) 33–40.
[54] C. Liu, B. Tang, S. Zhang, M. Zhou, M. Yang, Y. Liu, Z.-L. Zhang, B. Zhang, D.-W. Pang, Photoinduced electron transfer mediated by coordination between carboxyl on carbon nanodots and Cu^{2+} quenching photoluminescence, J. Phys. Chem. C 122 (2018) 3662–3668.
[55] L. Pan, S. Sun, L. Zhang, K. Jiang, H. Lin, Near-infrared emissive carbon dots for two-photon fluorescence bioimaging, Nanoscale 839 (2016) 17350–17356.